13th International Conference on
Structural Health Monitoring of Intelligent Infrastructure
DOI: 10.3217/978-3-99161-057-1-103

Practical approach to calibrating wireless sensors for use in structural health monitoring in an outdoor environment

Michael Markus Petschacher[1], Markus Krüger[1, 0000-0003-3364-7874]
[1]Institute of Technology and Testing of Construction Material, Faculty of Civil Engineering Sciences, Graz University of Technology, Inffeldgasse 24, 8010 Graz, Austria
email: petschacher@tugraz.at, krueger@tugraz.at

ABSTRACT: When sensor systems are used on outdoor structures (bridges, tunnels, etc.), they are exposed to a wide range of environmental influences. In particular, temperature can significantly affect the quality and accuracy of measurements. While most commonly available sensors are calibrated at temperatures of around 20°C before use, but the influence of variable temperatures is rarely considered. Furthermore, the measuring systems used for these sensors, particularly wireless sensor systems, are often only calibrated for room temperature. For this reason, this paper presents calibration procedures for monitoring systems including the sensors used (here displacement sensors are used as an example). The aim is to provide a practical routine for structural monitoring applications. This involves simulating typical temperature changes in a climate chamber (-20°C to +50°C) while measuring the temperature-induced strain of steel, and analyzing the reproducibility and temperature response of the entire measurement system. Other external influences affecting measurement quality are also discussed, and these are considered when determining the overall measurement uncertainty. This helps to define the requirements and limitations of measurement systems for structural health monitoring, particularly for bridges. The resulting findings should support the standardization process for assessing the suitability of monitoring systems for future SHM applications.

KEY WORDS: Calibration; Wireless Sensors; Environmental Influences.

1 INTRODUCTION

Structural Health Monitoring (SHM) plays a vital role in maintaining the long-term stability and safety of civil infrastructure. Among the various SHM technologies, wireless sensor networks (WSNs) have emerged as an efficient solution for the real-time monitoring of structural integrity. However, WSNs present specific challenges, particularly when deployed outdoors, where they are exposed to a variety of environmental factors. Bridges, for instance, are subject to extreme temperatures, rapid temperature fluctuations, wind, rain, and vibration, all of which can significantly affect sensor performance and measurement accuracy. Despite these challenges, most calibration efforts focus solely on the sensor itself and are typically performed under laboratory conditions at around 20°C. The effect of variable influences on the entire measurement system is often not sufficiently considered. These include not only external influences, but also aspects such as the stability of the measurement system in relation to its power supply (e.g., wireless sensors are often battery-powered). Such limitations can lead to measurement inaccuracies and impair the reliability of SHM systems in outdoor applications.

This paper presents the calibration process for a wireless monitoring system that measures displacement and strain. This system will later be used on a building to determine changes in strain or crack width with high precision. It should be noted that precision must be defined before selecting the appropriate sensors and sensor system. For example, in the context of service limit states, crack width change may require an accuracy of 0.05 mm. The proposed approach involves placing the complete sensor system in a climate chamber to simulate real-life temperature conditions and fluctuations ranging from -20 °C to +50 °C. Monitoring the temperature-induced strain of a steel plate under these controlled conditions enables the development of a more comprehensive and practical calibration routine for SHM applications.

It is expected that the findings of this research will enhance the accuracy and reliability of WSN-based SHM systems, particularly for bridges exposed to harsh environmental conditions, and to contribute to the standardization of calibration procedures in this field.

2 BACKGROUND AND BASICS

2.1 Wireless Sensor Systems in SHM Applications

WSNs for SHM offer a promising alternative to traditional wired sensor systems. The reliance on physical connections for power supply and data transmission in wired systems significantly increases the complexity, manufacturing costs and maintenance requirements of such systems. In contrast, wireless sensor systems integrate power supply or harvesting and wireless communication capabilities directly into the sensor units, enabling efficient data acquisition and real-time signal processing without the need for extensive cabling infrastructure. This self-sufficiency not only simplifies the deployment of SHM systems but also reduces the overall costs and logistical challenges associated with their maintenance [1].

WSNs can be applied to a variety of different use cases. The network usually consists of a series of motes (sometimes also referred to as nodes), each equipped with one or more sensors depending on the measurement task. For example, these sensors can measure temperature, humidity, strain, displacement, pressure, force, tilt, and other variables. The measured values are transmitted wirelessly to a central

DOI: 10.3217/978-3-99161-057-1-103

processing unit, which primarily stores and pre-processes the data. From there, the data is transmitted to the user for post-processing. It should be noted, however, that WSN applications are only of limited use for high-frequency measurements (vibrations, high-frequency load changes, etc.) due to the limited data transmission via radio and the limited energy supply in battery-powered WSNs (sampling rate correlates with energy consumption).

Figure 1 shows a standard schematic of a sensor mote, which can be described as having four major components: a sensor unit, a processing unit, a communication unit and a power supply unit [2]. When connecting analogue sensors, a suitable signal conditioning device and an analogue-to-digital (A/D) converter are also required.

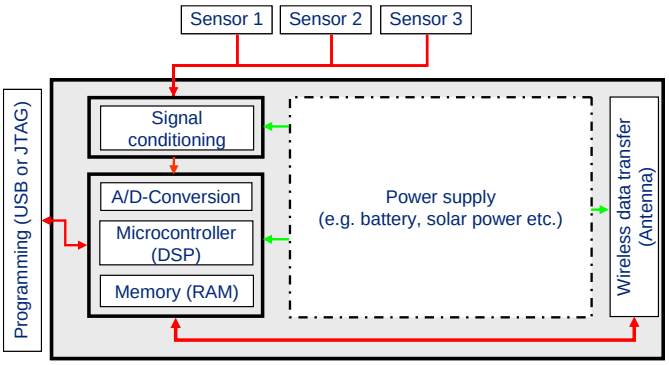

Figure 1. Block diagram of the hardware for a standard sensor mote [3].

While all these units vary depending on the application, they are subject to the same environmental influences when used outdoors. In this paper, the schematic in Figure 1 will be allocated with the components used in the calibration procedure and considered as a whole. Influences on the communication unit will not be discussed in order to focus on the sensors and the sensor mote themselves. Similarly, environmental influences on the power unit will not be considered, although fluctuations in the energy supply might affect the measurements.

2.2 External Influences on WSNs

A variety of external influences can affect both a wireless measurement system and the value being measured. As well as influences from the structure itself and how it is used (e.g. vibrations and deformations), environmental factors such as temperature and humidity also have a significant impact. The extent and nature of these influences depend largely on the structure's geographical location and the motes' specific positioning within it. It is essential to quantify these influences and take them into account when determining measurement results, as this is part of a highly recommended validation process.

For example, significant differences in environmental exposure can arise in the case of a bridge depending on whether sensors are mounted on the deck, beneath the structure, or within enclosed components such as hollow box girders. The Figure

primary influences affecting accuracy in wireless sensor systems can basically be categorized into two key factors, according to [3]:

- The transfer function between the physical quantity to be measured (stimulus) and the sensor system (specifically the sensor's response function). This defines how accurately and consistently the sensor converts the physical stimulus into a measurable signal.
- The cross-sensitivity of external disturbances on the measured quantity, which largely depends on the type of sensor and its underlying measurement principle. Such disturbances can introduce significant errors if not properly accounted for, particularly in environments with variable thermal, electromagnetic, or mechanical conditions.

Figure 2 shows an Ishikawa diagram of the many possible influences on a WSN node, which can impact the quality of the measurement. This categorization especially provides an overview of the basic influences, which are temperature [°K], relative humidity [%], shock [g1] and vibration [mm/s]. Depending on the location of the WSN, disturbances due to electromagnetic fields might also be a significant factor (for example, near high-voltage lines). More detailed documentation on the classification of electrotechnical components according to environmental influences can be found in EN 60721/IEC 721 multi-part standard series of the International Electrotechnical Commission (IEC).

This article only considers temperature as a decisive factor influencing the measured value determined by a wireless sensor and the calibration of the sensor system, as the influence of temperature is often not adequately determined during calibration by the manufacturer.

Since the temperature on external structures fluctuates greatly, some assumptions must be made. For example, the climate in a tunnel is more constant than on a bridge, where wind, solar radiation and humidity also play a role in addition to the air temperature. In order to determine upper and lower limits for the air temperature, statistical results for the area in question should be analyzed beforehand.

As an example, for Austria, according to the annual climate report in [4], the minimum air temperature in 2024 was measured at -25.5 °C in mountainous regions and -21.1 °C in urban areas, with a maximum temperature of +36.9 °C.

Another approach could be to use the temperatures used to calculate the integrity of the structure in question, which are mostly regulated in national standards. In case of the European standard in the national appendix, set in [5], a two-day average of the maxima and minima, appearing all 50 years, is used as the dimensioning value. There the lowest temperature expected is set for -32 °C in Austria, while the highest is set for smaller than +39 °C, depending on the sea level.

These values, as can also be seen in Table 1, provide a rough estimate of the required range.

2

[1] With [g] being a common unit for acceleration with 1 g being the gravitational acceleration of Earth: 1 g ≈ 9,81 m/s²

DOI: 10.3217/978-3-99161-057-1-103

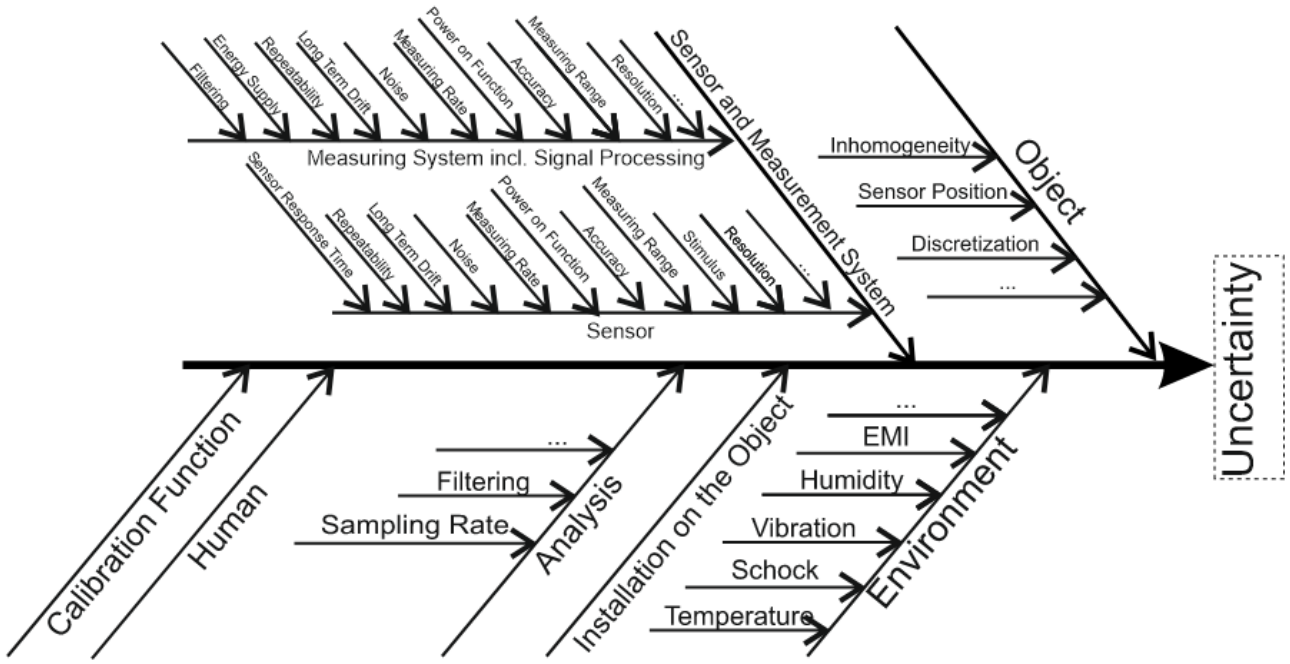

Figure 2. Ishikawa diagram showing the influences on the uncertainties of WSN nodes.

Table 1. Minima and maxima of air temperature in Austria.

Reference	T_{min} [°C]	T_{max} [°C]	ΔT [°K]
Austrian Measurement 2024	-25.5	36.9	62.4
Austrian Standard	-32	39	71

T_{min} … minimal temperature
T_{max} … maximal temperature
ΔT … difference of min and max

The examples in Table 1 do not apply to every case. Firstly, the effect of direct sunlight is not considered. Depending on the medium, surface temperatures near motes can be much higher, depending on the intensity of the sunlight. Secondly, the values shown are extreme pinpoints of the whole country. They can vary considerably depending on the location. Nevertheless, they demonstrate that the estimated temperature range that a WSN has to endure for long-term SHM, can exceed 60 K, ranging from below -10°C to above 30 °C, depending on various factors.

3 PROPOSED CALIBRATION METHODOLOGY

3.1 Experimental Setup

For experimental evaluation, an integrated sensor mote is placed in a climate chamber as a complete unit, including the sensors, but without the sensor mote housing. Approximately once per minute, measurement data is transmitted via a LoRa (Long Range) radio module to a receiver, which forwards the data to a remote database for storage and analysis.

The sensor mote provided by SmartMote [6] consists of two printed circuit boards (PCBs) and is referred to as Smartmote^{WS}. The primary PCB contains a microcontroller that is responsible for signal processing and data management. It also contains a communication interface (LoRa – 868 MHz), a power supply unit comprising two 3.6 V lithium thionyl chloride batteries, and several integrated measurement electronic components and digital sensors for measurement (see Figure 3). The second circuit board serves as a separate sensor interface card, which provides three ports for connecting analogue sensors. The card has a reference voltage and a voltage meter as well as 24-bit high precision analogue-to-digital conversion with adjustable gain for use with different sensor types (see Figure 4).

Table 2. Configuration of the Sensor Mote.

Sensor Mote Name:	SMUSE 143
Onboard measurements:	Acceleration x, y and z Temperature Relative humidity Battery voltage Illuminance
Port 1	Fixed resistors
Port 2	KG 2A – EFA231506
Port 3	KG 2A – EFA231507

Table 3. Specifications of the crack displacement transducers.

Transducer name	KG 2A – EFA231506
Capacity	2 mm
Rated Output	1480 µV/V (2960 x 10^{-6} strain)
Non-linearity	0,2 %RO
Input resistance	351.6 Ω

Transducer name	KG 2A – EFA231507
Capacity	2 mm
Rated Output	1430 µV/V (2860 x 10^{-6} strain)
Non-linearity	0,2 %RO
Input resistance	351.2 Ω

DOI: 10.3217/978-3-99161-057-1-103

For this experiment, the sensor interface board is equipped with two crack displacement transducers (model KG-2A, Tokyo Measuring Instruments Laboratory [7]), which are connected in a mirrored configuration to a steel plate (see Figure 6 and Table 4) to measure the thermally induced strain. Additionally, the third input channel is connected to a fixed resistor network, which acts as a stationary reference input to periodically validate the stability and performance of the measurement system under varying environmental conditions (see Table 2,

Table 3 and Figure 5 for technical details).

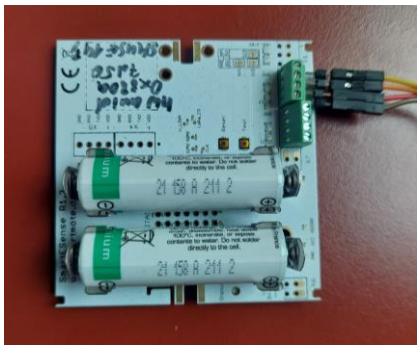

Figure 3. Primary PCB with power supply.

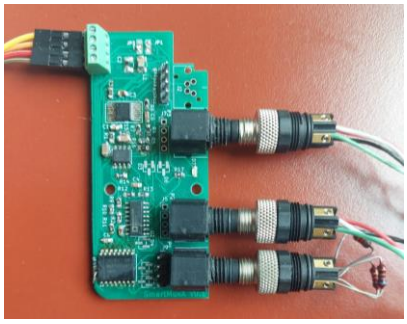

Figure 4. Secondary PCB with sensor ports.

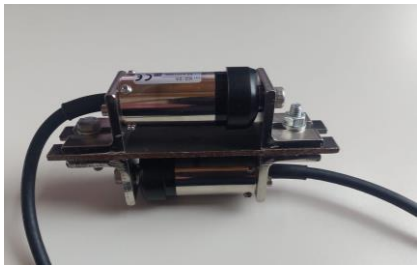

Figure 5. Crack displacement transducers on a steel plate.

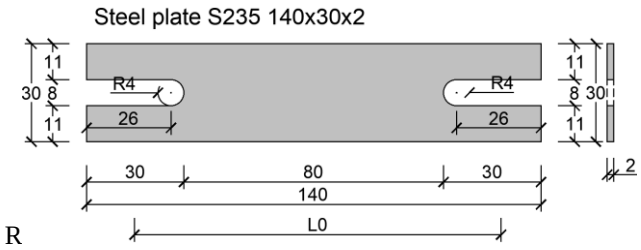

Figure 6. Steel plate S235 140x30x2 [mm].

A programmable climate chamber (model: VÖTSCH VT 4060) is used to determine the influence of environmental temperature variations. It allows precise temperature control within the range of -40°C to +180°C and includes adjustable ramp rates and programmable dwell times at set points. This enables reproducible temperature profiles to be implemented that are tailored to sensor calibration procedures.

Table 4. Characteristics of the steel plate.

Steel plate grade	S235 JR
Length	140 mm
Width	30 mm
Thickness	2 mm
Temperature coefficient α_T	~12*10^{-6} 1/°K
Base length of measurement L_0	103 mm

For the present calibration experiment, a temperature range of -20°C to +50°C is defined. This range is based on the boundary conditions discussed in section 2.2, with slight modifications to accommodate the technical limitations of the chamber. Although temperatures below -20 °C have historically occurred in the alpine regions of Austria, such extremes have become rare in recent years due to climate change. Conversely, +50°C approximates the extreme surface temperatures that can be experienced by bridge components exposed to direct sunlight in summer.

The temperature setpoints selected for this calibration are −20 °C, 0 °C, +20 °C, +35 °C, and +50 °C, as recommended in [3] for the thermal characterization of wireless sensor motes and their attached sensors. Each setpoint is maintained for 30 minutes to allow sufficient time for data collection and to determine the response time of the sensor system, as well as for statistical evaluation of repeatability. Thus, a minimum of five readings is taken at each plateau.

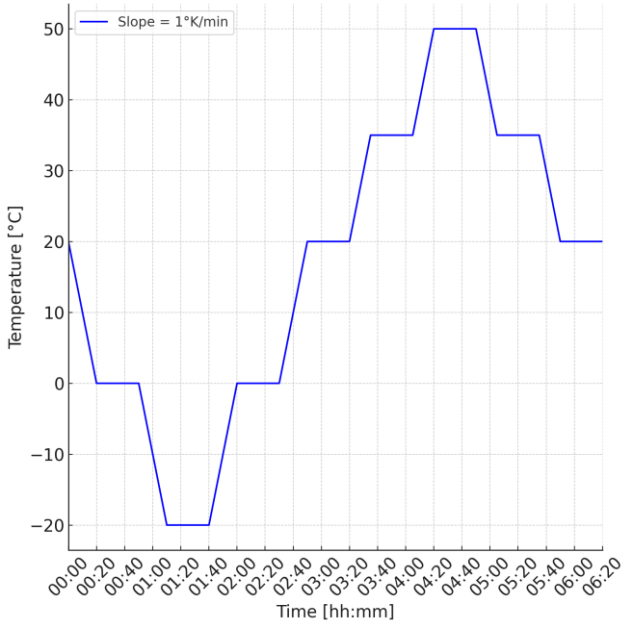

Figure 7. Temperature graph for one calibration cycle.

The full temperature profile is implemented as follows (see Figure 7 for the programmed profile): Starting from a reference temperature of +20 °C, the chamber performs a series of temperature ramps at a constant rate of 1 K/min. The temperature then drops to 0 °C, falls further to −20 °C, returns

DOI: 10.3217/978-3-99161-057-1-103

to 0 °C, rises to +20 °C, continues to +35 °C, and finally to +50 °C. It then returns to +20 °C via +35 °C. Each of these temperatures represents a holding period of 30 minutes.

This sequence defines one full temperature cycle, which is repeated ten times to increase the statistical significance of the results and to enable the observation of potential thermal hysteresis and time drift effects in the sensor system.

3.2 Calibration Procedure

To evaluate, calibrate and compare the performance of the two displacement sensors mounted on the steel plate (Figure 5), for which thermal expansion was calculated by using the chamber temperature and the characteristics of Table 4. It was decided to use ordinary structural steel for the application, rather than nickel-iron alloys (Invar steel) because the influence of steel strain on the uncertainty determination was expected to be minimal. Due to the homogeneous and predictable thermal expansion behavior of steel, its deformation under temperature change can be considered sufficiently uniform and it is therefore used as the "real" deformation value for comparison purposes.

The expected strain was calculated using the linear thermal expansion equation commonly applied in civil and structural engineering for practical application. The strain induced by temperature is defined as:

$$\Delta l = \alpha_T * \Delta T * l_0 \quad (1)$$

with:

Δl : absolute elongation or contraction [mm]
α_T : coefficient of linear thermal expansion [1/°K]
ΔT : temperature difference relative to a reference [°K]
l_0 : original base length of measurement [mm]

For this experimental setup, the reference temperature is 20 °C and the base length of the steel segment between the two sensors is l_0 = 103 mm. The coefficient of linear thermal expansion for structural steel is assumed to be $\alpha T = 12*10^{-6}$ 1/°K (Table 4) with an assumed standard deviation of ~$0{,}3*10^{-6}$ 1/K. The expected median deformation values for the two temperature extremes in the calibration protocol are calculated using equation (1):

- Maximum elongation at +50 °C (ΔT = +30 K):
  $\Delta l = 12\ (\pm 0.3) \times 10^{-6} \times 30 \times 103 =$ 0.037 (±0,001) mm
- Maximum shortening at −20 °C (ΔT = −40 K):
  $\Delta l = 12\ (\pm 0.3) \times 10^{-6} \times (-40) \times 103 =$ −0.049 (±0,001) mm

The calculated values serve as a reference line for the evaluation of the measurement results of both sensors. When functioning correctly, the cumulative deformation values recorded by the sensors should closely follow this curve, assuming a uniform temperature distribution and negligible mechanical disturbances.

The calibration procedure involves repeating the temperature cycle described in section 3.1 six times. During each cycle, measurements are recorded at a sampling rate of approximately one measurement per minute. It should be noted that this interval is shorter than is typical for long term monitoring applications, and therefore occasional inconsistencies in the data are to be expected as the system is optimized for lower frequency measurements.

Following the temperature programming, the sensors are subjected to controlled thermal load in the climate chamber. The measurement output consists of a differential voltage signal relative to a reference voltage, which is continuously recorded and transmitted via the wireless mote system. A calibrated transfer function is then used to convert this voltage output into a displacement in millimeters [mm].

This conversion is based on the known sensitivity characteristics of the strain gauges (

Table 3), and the applied formula as shown in Equation (2):

$$X = \frac{main_{mvpv}}{(1000 - ref_{mvpv}) \cdot \frac{R_{sensor}}{R_5}} \cdot \frac{Cap_{sensor}}{RO_{Sensor}} \cdot 1000 \quad (2)$$

with:

X calculated displacement [mm]
$main_{mvpv}$ measured voltage at the sensor output [mV/V]
ref_{mvpv} reference voltage equal to all supply voltages of the components [mV/V]
R_5 reference resistance of the measurement system being 100 in the apparent setup [Ω]
R_{sensor} input resistance of the Wheatstone Bridge of the used sensor [Ω]
RO_{Sensor} characteristic value of the Wheatstone bridge for the measuring range [mV/V]
Cap_{Sensor} measuring span of the used sensor [mm]

Based on this formula, a data structure (see Table 5) is generated. To align the time domains of the two systems, the temperature measurements from the climate chamber are linearly interpolated to match the timestamps of the wireless sensor node. Figure 8 shows the results of the measurements at the set temperatures. The calculated cumulative displacement is set to zero for the first measurement at 20°C.

Table 5. Data structure of experiment.

Column name	Description
__time	Datetime of the measurement [YYYY-MM-DD hh:mm:ss]
Ref_mV_per_V	reference voltage equal to all supply voltages of the components [mV/V] (see equation (2))
mV_per_V	measured voltage at the sensor output [mV/V] (see equation (2)
Displacement	Calculated displacement of each timestep in [mm] (see equation (2)
Delta displacement	Calculated displacement subtracted from each timestep before in [mm]
Cumulative displacement	Cumulative displacement started with the first timestep as zero in [mm]
Temperature	Measured temperature of the climate chamber interpolated for each measured timestep in [°C]
Reference temperature	Temperature which is programmed for the cycle (not measured) in [°C]
Cycle direction	Differentiated into cooling, heating and constant
Steel	Expected displacement of the steel plate with ideal strain in [mm] (see equation (1))
Error	Difference of cumulative measurement and steel in [mm]

DOI: 10.3217/978-3-99161-057-1-103

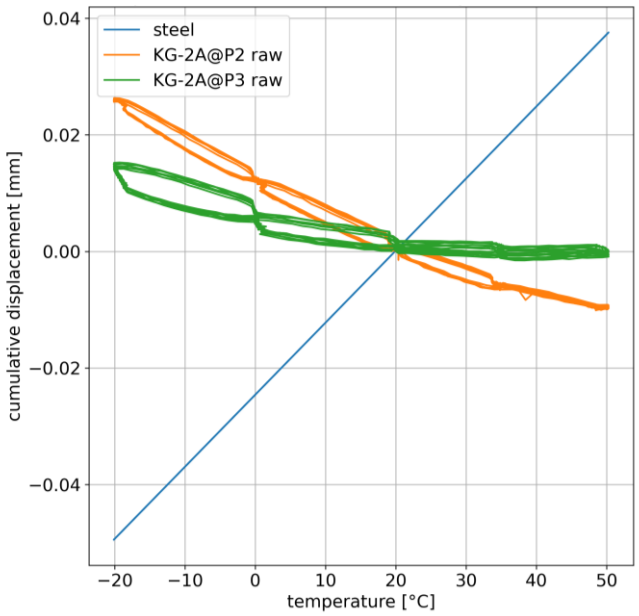

Figure 8. Raw data of cumulative displacement for both displacement transducers.

Figure 8 shows the results of the cumulative displacement of the two KG-2A sensors (Port 2 and Port 3) plotted against the temperature profile of the climate chamber and the theoretical elongation of the steel reference. Neither of the two sensor curves matches the expected thermal elongation of steel (blue line), which indicates a systematic error in the raw measurement data.

During heating and cooling phases, both sensors follow different curves. However, at the holding points where the temperature was kept constant, the cumulative displacement of both sensors converge to a common value. This behavior suggests that the response time of the sensors may need to be considered when higher accuracy requirements are specified.

3.3 System Temperature Compensation

It has not yet been clarified whether the measurement error (Figure 8) is due to the sensors themselves or to the measurement system. In order to isolate and correct the systematic temperature sensitivity of the wireless mote itself, a special reference arrangement was implemented using a full Wheatstone bridge composed of high precision 350 Ω (0.1%) resistors, which were connected to Port 3 of the sensor mote. This configuration allows sensor specific strain effects to be excluded and ensures that only thermal influences on the measurement electronics are detected.

The entire system was placed into the climate chamber and subjected to the same thermal cycling protocol. Since the strain gauges in the KG-2A sensors also operate with a Wheatstone bridge of approx. 350 Ω, this setup simulates the electrical behavior of such a sensor. Consequently, all recorded voltage variations can be attributed solely to temperature-related shifts in the signal conditioning circuit.

A correction function can therefore be derived from the resulting data set, which can be used to compensate the systematic temperature error of the wireless measurement system. This step is essential for improving measurement accuracy in an outdoor environment.

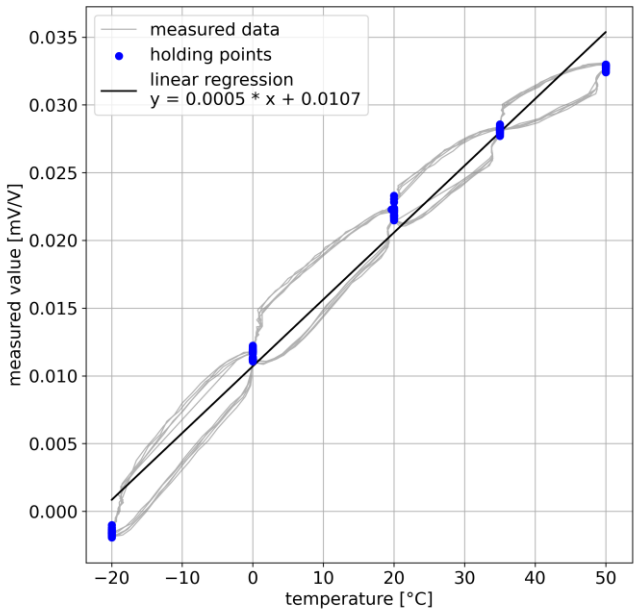

Figure 9. Results for the 350 Ω reference arrangement and linear regression for temperature compensation.

Figure 9 shows the results for the 350 Ω reference arrangement connected to Port 3. As can be seen, there is a systematic error in the measurement system over the investigated temperature range. To quantify the systematic thermal influence of the mote, a linear regression model was developed based on the stabilized measurement data at the holding points. Specifically, the final ten data points at each temperature plateau were extracted, equivalent to the final ten minutes of each holding phase. This time window was chosen to ensure that the system had reached thermal equilibrium, thereby minimizing transient effects caused by sensor response delays. The resulting data was used to fit a linear correction function with temperature as the independent variable, as shown in the following equation (3) below:

$$main_{corr} = main_{mvpv} - 0{,}0005 * T - 0{,}0107 \quad (3)$$

with:

$main_{corr}$	corrected measurement [mV/V]
$main_{mvpv}$	measured voltage at the sensor output [mV/V]
T	measured temperature [°C]

The corrected measurement is then inserted back into equation (2) to calculate the corrected displacement. The results of the corrected measurements can be seen in Figure 10 exemplary for KG-2A on Port 3.

As shown in Figure 10, correcting the error caused by the measuring system reduces the absolute error, but it is still relatively large. The deviation from the ideal strain curve of the steel is most likely due to the design of the sensor. The sensor itself consists largely of a steel construction, with the Wheatstone bridge presumably implemented inside the sensor via a type of spring mechanism. The steel construction therefore deforms almost identically to the steel rail in response to temperature, so that the Wheatstone bridge does not experience any significant strain.

DOI: 10.3217/978-3-99161-057-1-103

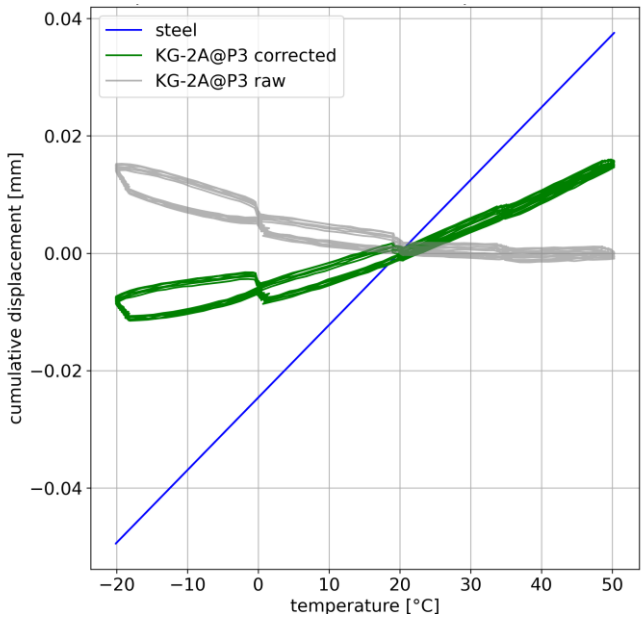

Figure 10. Corrected values on KG-2A@Port 3.

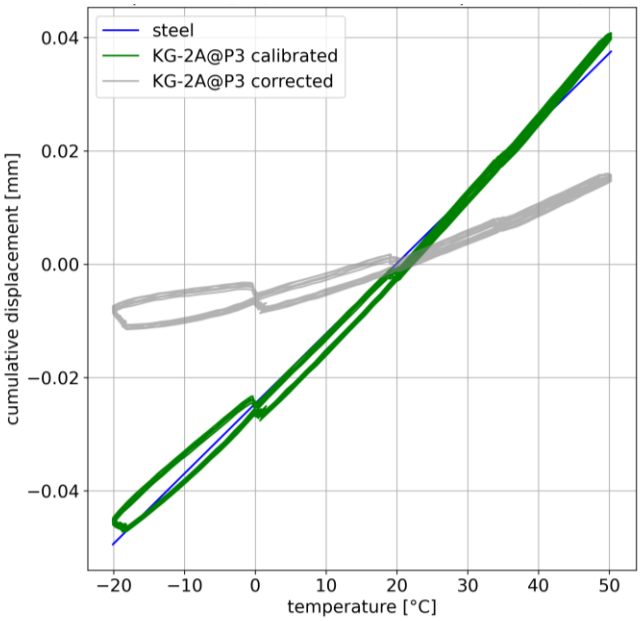

Figure 11. Calibrated displacements on KG-2A@Port 3.

3.4 Sensor Temperature Compensation

The procedure for temperature compensation of the sensors is carried out in the same way as for determining the correction function for the temperature error caused by the measuring system. A linear regression over the last ten measurements at each hold point forms the basis for the correction formula for each individual sensor. The linear change in length of the steel plate is then also calculated using a linear function. From these two, a correction function (4) is created with temperature as the independent variable in order to calibrate the sensor with regard to its temperature behavior.

$$X_{cal} = X_{raw} + \left(k_{steel} - k_{lin.reg.}\right) * \mathrm{T} - \left(d_{steel} - d_{lin.reg.}\right) \quad (4)$$

with:

X_{cal}	calibrated displacement [mm]
X_{raw}	corrected displacement acc. to equation (2) [mm]
k_{steel}	slope of the steel function [0.00123]
$k_{lin.reg.}$	slope of the linear regression of the raw measurements [0.0003]
T	measured temperature [°C]
d_{steel}	intercept of the steel function [-0.0244]
$d_{lin.reg.}$	intercept of the linear regression of the raw measurements [-0.0048]

Following calibration, the corrected measurement data clearly shows a trend towards the expected thermal elongation of the steel reference, as demonstrated in Figure 11 for the KG-2A sensor connected to Port 3.

3.5 Uncertainty Analysis

The uncertainty analysis involves evaluating each input parameter according to the classification defined in [8], distinguishing between Type A and Type B uncertainties. This procedure is also described for a comparable experiment in [9]. Type A evaluation is based on the statistical analysis of repeated measurements and is applied to the cumulative measurement value in this setup. Type B evaluation, on the other hand, relies on scientific judgement or prior information. Accordingly, the uncertainty associated with the elongation of the steel for example is classified as Type B. For practical purposes, the temperature is considered ideal. Consequently, rather than the actual temperature measured by the sensor mote, the temperature of the climate chamber (see Table 5) is used as a reference for this analysis.

Furthermore, the displacement calibration performed on a similar KG-2A sensor from [10] will be taken into account as an example.

Measurement error:

The measurement error is included in the data structure in Table 5 and is calculated using the following equation (5):

$$\varepsilon(t,T) = \Delta l_{measured}(t) - \Delta l_{steel}(T) \quad (5)$$

with:

$\varepsilon(t)$	error for each timestep [mm]
$\Delta l_{measured}(t)$	calibrated cumulative measurement for each timestep [mm]
$\Delta l_{steel}(T)$	expected steel elongation for each temperature [mm]

Type A uncertainty:

For the evaluation of Type A uncertainty, the methodology outlined in ([8], p. 22) is applied to each sensor port individually. This analysis assumes that the measurement deviations approximately follow a Gaussian (normal) probability distribution, which is a reasonable approximation for random fluctuations in sensor readings under stable

DOI: 10.3217/978-3-99161-057-1-103

conditions. The arithmetic mean and the experimental standard deviation of the measurement error are calculated from the last ten measurements at each holding point to account for sensor response time. This allows for a detailed quantification of the repeatability and consistency of the sensor system under varying thermal conditions. Mathematically, the Type A uncertainty is expressed as follows:

$$u_i = s = \sqrt{\frac{1}{n-1}\sum_{i=1}^{n}(x_i - \bar{x})^2} \quad (6)$$

With:

x_i	individual error values in [mm]
$\bar{x}$	mean error
s	sample standard deviation, representing the Type A uncertainty

Following the Type A uncertainty evaluation for each port as shown in Table 6, Figure 12 illustrates the calibrated error including the standard deviation for each temperature holding point. Also shown in Table 6 is the final unweighted mean error and corresponding deviation across the entire temperature span. Figure 12 shows the error bands for raw, corrected, and calibrated data, highlighting the effect of each correction stage on measurement uncertainty.

Table 6. Type A uncertainty for each temperature holding point, after temperature compensation.

Temperature	KG-2A@Port2		KG-2A@Port3	
[°C]	$\bar{x}$ [mm]	s [mm]	$\bar{x}$ [mm]	s [mm]
u_{t-20}	0.0033	0.0002	0.0039	0.0004
u_{t0}	-0.0004	0.0002	-0.0011	0.0005
u_{t20}	-0.0020	0.0003	-0.0020	0.0006
u_{t35}	-0.0008	0.0004	-0.0001	0.0007
u_{t50}	0.0037	0.0002	0.0029	0.0004
u_{temp_full}	0.00076	0.0001	0.00072	0.0002

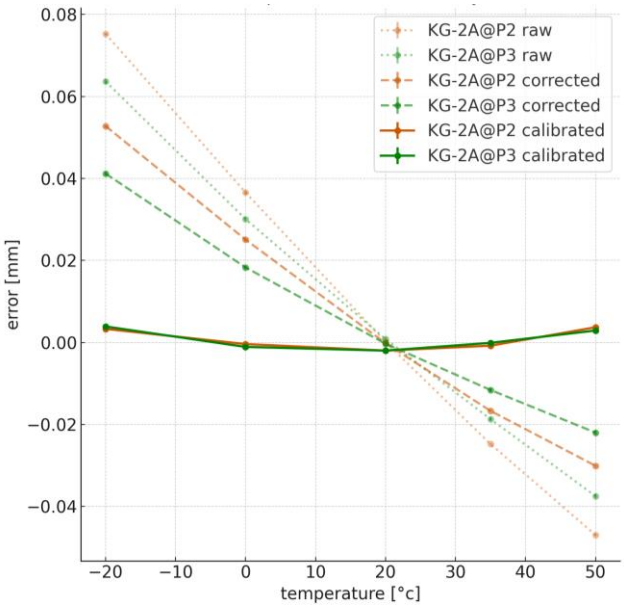

Figure 12. Error diagram for raw and compensated values.

The mean error at each holding point should be interpreted as a systematic bias (or also known as truthfulness) relative to the assumed real value. Since the total mean value of the errors across all temperatures after temperature compensation is relatively low, it is not considered in further uncertainty calculations. The decisive factor for the uncertainty assessment is therefore solely the combined consideration of the uncertainties at each hold point.

Type B uncertainty:

In accordance with the methodology described in [[8], p. 23], Type B uncertainty is evaluated based on input quantities whose variability is derived from scientific judgement, manufacturer specifications or published data, rather than from repeated observations. As the aim of this paper is to establish a practical and field-adaptable calibration approach, not all parameter uncertainties are derived from formal traceable standards. Nevertheless, the main sources of Type B uncertainty in this setup are clearly identified and justified. Three factors are shown: the variance of the temperature coefficient of steel αT, assumed to be ±0,3*10-6 1/°K, the nonlinearity of each sensor (shown in

Table 3) and the displacement calibration given from an earlier analysis for a KG-2A sensor [10]. Given the variance of αT for a base length of 103 mm and a base temperature of 20°C the uncertainty of the elongation for every holding point is shown in Table 7 (calculated using Equation (1)).

Table 7. Uncertainty of elongation at holding points by variance of steel temperature coefficient.

Uncertainty by Temperature	s [mm]
$u_{steel\ -20}$	0,0012
u_{steel0}	0,0006
$u_{steel20}$	0
$u_{steel35}$	0,00046
$u_{steel50}$	0,00092

According to the manufacturers' datasheet for the displacement sensors [7], the nonlinearity is specified as 0.2 % of the rated output (RO). Given the full-scale measurement range of ±2 mm (i.e., a total span of 4 mm), the resulting nonlinearity can be interpreted as contribution to the uncertainty of $u_{RO} = 0.002 \times 4\ mm = 0.008\ mm$. However, the datasheet does not provide further details regarding the determination of this nonlinearity or whether the 0.2 % RO represents a standard uncertainty or a combined uncertainty with a coverage factor (e.g. k=2). Therefore, in the absence of this information, the nonlinearity is conservatively treated as a Type B uncertainty contribution in accordance with the GUM framework.

Additionally, prior calibration using a similar KG-2A displacement sensor yielded a calibration uncertainty of $u_{dis\text{-}cal} = 0.003\ mm$ based on measurements within a range of ±1.5 mm. As no significant nonlinear behavior is expected beyond this range and there is no evidence to suggest otherwise, the same calibration uncertainty is assumed to be valid over the full range of ±2 mm. This assumption is also incorporated into the Type B uncertainty budget.

The complete Type B uncertainty is calculated using equation (7) for general purposes and equation (8) for this demonstration, with the results shown in Table 8:

DOI: 10.3217/978-3-99161-057-1-103

$$u_B = \sqrt{\sum_{i=1}^{n} u_i^2} \quad (7)$$

$$u_B(T) = \sqrt{u_{\alpha T}^2(T) + u_{RO}^2 + u_{dis-cal}^2} \quad (8)$$

with:

u_B combined uncertainty for Type B
u_i individual uncertainty of each factor falling in Type B, $u_{\alpha T}(T)$ is the variation of the steel elongation depending on the temperature coefficient
u_{RO} nonlinearity given by the datasheet
$u_{dis-cal}$ evaluated uncertainty due to displacement calibration

Table 8. Type B uncertainty by temperature.

Type B by Temperature	s [mm]
u_{B-20}	0.0086
u_{B0}	0.0086
u_{B20}	0.0085
u_{B35}	0.0086
u_{B50}	0.0086
$u_{Btemp-full}$	0.0086

Table 8 shows that the influence of uncertainty on the temperature coefficient is irrelevant in this experiment and will therefore not be discussed any further.

Combined uncertainty:

The combined standard uncertainty u_c is derived by aggregating the individual contributions of Type A and Type B uncertainties. Type A uncertainty reflects the statistical dispersion in repeated measurements, while Type B uncertainty accounts for systematic influences, such as variations in material properties and sensor nonlinearity. Assuming that these contributions are uncorrelated, the combined uncertainty is calculated using the root-sum-of-squares method, as recommended by the GUM framework [8]:

$$u_C = \sqrt{u_A^2 + u_B^2} \quad (9)$$

Substituting the Type A and Type B values for this experiment into Equation (9) the combined uncertainty for this setup is given in Table 9. It shows that for the temperature compensated values the uncertainty is determined by the factors of Type B.

Table 9. Combined uncertainty of the sensors on both ports.

	KG-2A@P2			KG-2A@P3		
[°C]	u_A [mm]	u_B [mm]	u_C [mm]	u_A [mm]	u_B [mm]	u_C [mm]
-20	0.0002		0.0086	0.0004		0.0086
0	0.0002		0.0086	0.0005		0.0086
20	0.0003	0,0086	0.0086	0.0006	0,0086	0.0086
35	0.0004		0.0086	0.0007		0.0086
50	0.0002		0.0086	0.0004		0.0086
Full Span	0.0001	0.0086	0.0086	0.0002	0.0002	0.0086

If the values for Type A and Type B for this experiment are inserted into equation (9), the combined uncertainty is obtained as shown in Table 9. It can be seen that the combined uncertainty for the temperature-compensated values is essentially determined by the Type B uncertainties.

Expanded uncertainty:

To express the measurement uncertainty with a defined level of confidence, the expanded uncertainty U is calculated by multiplying the combined standard uncertainty u_C by a coverage factor k as shown in Equation (10):

$$U = k * u_C \quad (10)$$

with:

U expanded uncertainty
k coverage factor chosen with
u_C combined uncertainty

In this study, a coverage factor of k=2 is applied, which corresponds to an approximate 95% confidence level under the assumption of a normal distribution, as recommended in [8]. The resulting expanded uncertainty, as shown in Table 10, defines an interval around the measurement result within which the true value is expected to lie with a high degree of probability. This value is crucial for ensuring the reliability of decision thresholds and condition assessments in the presence of measurement variability, and serves as a practical limit for interpreting sensor data in structural health monitoring applications.

Table 10. Expanded uncertainty of the sensors on both ports

	u_C [mm]	U [mm]
KG-A2@Port 2	0.0086	0.0172
KG-A2@Port 3	0.0086	0.0172

4 DISCUSSION AND RESULTS

Previous studies have shown that sensor systems exposed to temperature fluctuations can exhibit irregular and inconsistent behavior with regard to the measured value to be recorded. In the present study, laboratory tests with wireless displacement sensors under the influence of temperature are carried out as examples. The displacement sensors are fixed to a steel plate in order to simulate guided deformation similar to an application on steel or reinforced concrete components with similar thermal expansion behavior.

Measurements (Figure 8) with wireless sensor nodes and displacement sensors have shown that the raw data on deformation deviates significantly from the expected thermal deformation of the steel. In addition, a temperature-dependent sensor response was observed during heating and cooling, which raises the question of how temperature influences and gradual changes can be handled and compensated for in on-site applications. Since convergence and reproducibility are achieved at different temperature holding points, it is possible to perform temperature compensation. In the present case, linear temperature compensation proved to be suitable for compensating for the influences from both the measuring system itself and the connected sensors. However, such temperature compensation is only possible if the sensors stabilize at a consistent value after reaching thermal

DOI: 10.3217/978-3-99161-057-1-103

equilibrium. A special feature here is that the sensors under investigation themselves exhibit temperature expansion, which overlaps with the deformation to be measured on the component. It is therefore relatively difficult to carry out highly accurate measurements if the sensor temperature and the component temperature are unknown or even different, which can certainly occur in practice. This is particularly important when displacement transducers and discrete measuring paths of several centimeters are used to measure crack width changes in the hundredth of a millimeter range, as sensor and component expansion accompany the change in crack width. The same applies when displacement transducers are used to determine expansion with accuracies of approximately 10 µstrain. This article has explained that the influences on measurement uncertainty can be very diverse. These range from measurement uncertainties of the measuring system itself, including uncertainties from the power supply, to uncertainties of the connected sensors, to measurement uncertainty regarding the sensor mounting on the object and a wide range of other external influences.

In order to quantify and correct the influence of the measuring system, a special reference arrangement with a Wheatstone bridge consisting of identical high-precision resistors was implemented. This setup, which excludes mechanical components and deformations, shows the inherent temperature sensitivity of the mote and serves as the basis for a sensor node-specific correction function that ultimately also includes the individually connected sensors. For this purpose, temperature compensation functions were derived based on measurements at different temperature plateaus and measurement uncertainties were determined.

A comprehensive uncertainty analysis based on the GUM framework shows that, after calibration, the dominant contribution to the total uncertainty is of type B, provided that the uncertainty contribution of type A could be significantly reduced by applying temperature compensation functions (determined by calibration in temperature change tests). The final expanded measurement uncertainty for the measurement system shown with two displacement sensors is therefore less than 0.02 mm (20 µm), whereby without temperature compensation, a measurement uncertainty of at best approximately 50 to 100 µm can be assumed, depending on the temperature range.

CONCLUSIONS

An important finding was that the thermal response of the sensor housing and mounting components largely matched that of the monitored steel structure. This resulted in a partial cancellation of thermally induced displacement, which highlights the need for proper system calibration and temperature compensation. A correction function derived from a temperature-controlled reference experiment and validated using stable measurement intervals effectively reduced systematic errors and extended uncertainty to less than 20 µm. Furthermore, the comparison of the two identically installed sensors revealed distinct response behaviors in the raw measurements. This indicates that in this case individual calibration is recommended for each sensor, rather than relying on batch calibration procedures.

This study emphasizes the importance of considering the sensor and its mechanical integration as a unified measurement system. By demonstrating a reproducible calibration routine that considers electronic, mechanical and environmental influences, this study contributes to the practical standardization of wireless SHM devices. It therefore represents a step forward in providing information on the accuracy of sensors and sensor systems under real-world conditions. In the past, this was often not sufficiently taken into account, leading to misinterpretations of the measured values.

REFERENCES

[1] A. Deivasigamani, A. Daliri, C. H. Wang and S. John., A Review of Passive Wireless Sensors for Structural Health Monitoring, Modern Applied Science Vol. 7, No. 2 ISSN 1913-1844, http://dx.doi.org/10.5539/mas.v7n2p5, (2013).

[2] Siew, Zhan & Wong, Chen & Kiring, Aroland & Chin, Renee & Teo, Kenneth. (2012). Fuzzy logic based energy efficient protocol in wireless sensor networks. ICTACT J. Commun. Technol. (IJCT). 3. 639-645. 10.21917/ijct.2012.0091.

[3] M. Krüger, W. Lienhart, Präventives Bauwerksmonitoring mit intelligenten, vernetzten Systemen PreMainSHM: Leitfaden Bauwerksmonitoring, Graz, Austria, (2025).

[4] GeoSphere Austria, 2024: Monatlicher Klimabericht Österreich für das Jahr 2024, Vienna, Austria, 2025 URL: https://www.zamg.ac.at/zamgWeb/klima/klimarueckblick/archive/2024/wiewars24.pdf (2024)

[5] Austrian Standards International. ÖNORM B 1991-1-5: Allgemeine Einwirkungen – Temperatureinwirkungen, Wien: Austrian Standards International, 2012.

[6] TTI GmbH – TGU Smartmote, URL: https://smartmote.de/joomla/de/, Stuttgart, 2025

[7] TML – Tokio Measuring Instruments Laboratory, URL: https://tml.jp/e/product/transducers/kg.html, Tokio, 2025

[8] BIPM, IEC, IFCC, ILAC, ISO, IUPAC, IUPAP, and OIML. Evaluation of measurement data — Guide to the expression of uncertainty in measurement. Joint Committee for Guides in Metrology, JCGM 100:2008. doi:10.59161/JCGM100-2008E.

[9] Zhao Y, Zhang F, Ai Y, Tian J, Wang Z. Comparison of Guide to Expression of Uncertainty in Measurement and Monte Carlo Method for Evaluating Gauge Factor Calibration Test Uncertainty of High-Temperature Wire Strain Gauge. Sensors (Basel). 2025 Mar 6;25(5):1633. doi: 10.3390/s25051633. PMID: 40096503; PMCID: PMC11902841.

[10] H. Pongratz, IMBT-TU Graz, Calibration of displacement sensor KG-2A, 2023